Carbon nanotube localization at interface in co-continuous blends of polyethylene and polycarbonate

Riho Nishikawa[1)], Kakeharu Tamaki[1)], Osamu Notoya[2)],

and Masayuki Yamaguchi[1)]*

1) School of Materials Science, Japan Advanced Institute of Science and Technology, 1-1 Asahidai, Nomi, Ishikawa 923-1292, JAPAN

2) Center for Nano Materials and Technology, Japan Advanced Institute of Science and Technology, 1-1 Asahidai, Nomi, Ishikawa 923-1292, JAPAN

*Corresponding author:
E-mail address: m_yama@jaist.ac.jp (Masayuki Yamaguchi)
Phone: +81-761-51-1621
Fax: +81-761-51-1149

ABSTRACT

A new technique to show good electroconductivity was proposed using carbon nanotube (CNT) localization in co-continuous immiscible polymer blends comprising ultra-high-molecular-weight polyethylene (UHMWPE) and polycarbonate (PC). When UHMWPE was added to PC/CNT in the molten state in an internal mixer, CNTs started moving to the UHMWPE phase. However, CNTs require a long time to diffuse into the UHMWPE phase owing to a low diffusion constant. Consequently, they remain at the interface between PC and UHMWPE. When the blends have co-continuous structure, the localized CNTs at the phase boundary act as a conductive path, leading to a good electroconductivity. Although a similar morphology is obtained by adjusting the balance of interfacial tensions among polymers and CNT, it is difficult to find a system showing appropriate interfacial tensions. Since the present method is applicable to various polymer blends, it will be an important technique to prepare a conductive nanocomposite.

Keywords: Polymer blend; Co-continuous structure; Electroconductivity; Carbon nanotube

INTRODUCTION

The most obvious aim when formulating polymer nanocomposites containing conductive fillers is electroconductivity. When a composite comprises a single polymer species and a conductive filler, the conductivity is determined by the dispersion of the filler in the polymer, by the shape and size of the filler particles[1-5] —as described by the percolation theory[6,7]—and by the conductive performance of the filler itself. In the case of a polymer blend with a phase-separated structure, good conductivity is obtained with a relatively small amount of fillers when the matrix phase has a conductive path. This phenomenon is called double percolation and employed in various systems these days.[8-13] When in equilibrium, filler dispersion is determined by the balance of interfacial tensions $\Gamma_{i\text{-}j}$ between i and j, i.e., the thermodynamic effect, which is described by the wetting coefficient ω_a as follows:[14,15]

$$\omega_a = \frac{\Gamma_{A-Filler} - \Gamma_{B-Filler}}{\Gamma_{A-B}}. \quad (1)$$

When ω_a is smaller than -1, fillers exist in polymer A. In contrast, fillers remain in polymer B when $\omega_a > 1$. Moreover, they are localized at the interface when $-1 < \omega_a < 1$.

Nanofiller localization also results from kinetic effect.[10,16-22] Lee et al.[16] prepared a conductive rubber sheet by compression molding of small rubber particles on which conductive fillers were coated. In this system, the slow diffusion of nanoparticles into the rubber is responsible for creating a conductive path. A similar technique was proposed by Chan et al.,[17] Zhang et al.,[19] and Jia et al.[10] using ultra-high-molecular-weight polyethylene (UHMWPE), and by Grunlan et al.[18] using latex rubber. Recently, Wu et al.[21] employed this technique for a blend containing polypropylene (PP), and Zheng et al.[22] used it for a thermoplastic elastomer obtained by the dynamic vulcanization method. These reports demonstrated that the distribution of nanofillers in a polymer blend with phase separation is often different from the equilibrium one owing to the high viscosity of such blends. When a nanofiller has a low interfacial tension with respect of a high-viscosity polymer, it must reside on the surface of the

high-viscosity phase. Such localization in co-continuous structures enables the formation of an electrically conductive path with a significantly small amount of conductive fillers.

Carbon nanotubes (CNTs) are one of the best-known conductive nanofillers.[23-29] The interfacial tension Γ with a polymer can be estimated by the Girifalco-Good equation[30,31] from the surface free energy γ.

$$\Gamma_{1-2} = \gamma_1 + \gamma_2 - 2\sqrt{\gamma_1\gamma_2}\,. \quad (2)$$

The surface free energy of CNT, which must be affected by the production method, was reported to be 45.3 [mN/m][32] and 78.4 [mN/m][33]. The values are much higher than those of most conventional plastics, e.g., 25.4 [mN/m] for polyethylene (PE) and 32.1 [mN/m] for polycarbonate (PC) at 200 °C,[34] leading to $\omega_a > 1$ or $\omega_a < 1$. Therefore, CNTs often stay in one phase in an immiscible polymer blend. In the case of PE/PC blends, it is predicted that CNTs are dispersed in the PC phase. In a previous study, however, it was found that multi-walled carbon nanotubes (MWCNTs) are preferentially dispersed in high-density polyethylene (HDPE) in a phase-separated blend of PC and HDPE.[35] Moreover, MWCNTs were dispersed in ethylene–propylene copolymer (EPR) droplets in a blend of PP and EPR.[36] These results are attributed to the adsorption of HDPE and EPR molecules on the MWCNT surfaces during melt mixing. Furthermore, HDPE molecules were adsorbed on the MWCNTs more readily than EPR, suggesting that the ethylene unit is responsible for surface adsorption.[35,37] The surface adsorption was accelerated by high-temperature mixing, presumably owing to the frequent generation of radicals. These results demonstrate that bound molecules generated during mixing play an important role in nanofiller distribution.

In the present study, UHMWPE, instead of HDPE, was employed with PC as polymer species. According to the previous researches on PC/HDPE blends,[35,37] CNTs were homogeneously distributed in the HDPE (molecular weight = 4.9 x 10^4) phase as a result of the surface adsorption. In the case of the present system using UHMWPE (molecular weight = 3.3

x 10^6), the diffusion constant of CNTs in the UHMWPE, which is inversely proportional to the polymer viscosity,[38] is much lower than that in the HDPE. As a result, they accumulated at the interface, providing good electroconductivity when a blend has a co-continuous structure.

When the interphase localization of nanofillers is attained by the thermodynamic effect; i.e., balance of interfacial tensions among polymers and CNTs, we have to select only restricted systems having $-1 < \omega_a < 1$. Furthermore, the interfacial tension between a polymer and CNT ($\Gamma_{i\text{-}CNT}$) is usually much higher than that between different polymers ($\Gamma_{A\text{-}B}$). Therefore, most immiscible polymer pairs cannot satisfy the requirement of ω_a to be localized at phase boundary. In other words, only an immiscible blend having a large interfacial tension ($\Gamma_{A\text{-}B}$), leading to coarse morphology, can have CNTs at the boundary. Of course, such blends usually show poor mechanical properties. Therefore, the technique presented in this paper should be noted as a novel method to obtain a conductive polymer composite.

MATERIALS AND METHODS

Materials

The following commercially available polymers were employed in this study: Panlite L-1225Y bisphenol A polycarbonate (PC) (melt mass-flow rate (MFR) = 11 g/10 min; Teijin Ltd., Japan) and UH900 ultra-high-molecular-weight polyethylene (UHMWPE) (Asahi Kasei Corp., Japan). The number- and weight-average molecular weights of the PC—characterized by an HLC-8020 size exclusion chromatography (SEC) (Tosoh Corp., Japan) using chloroform as an eluent and a polystyrene standard—were $M_n = 1.9 \times 10^4$ (Da) and $M_w = 9.7 \times 10^4$ (Da), respectively. The average molecular weight of the UHMWPE, according to its intrinsic viscosity, was 3.3×10^6 (Da). The densities of the PC and the UHMWPE at 23 °C were 1200 kg/m^3 and 940 kg/m^3, respectively.

A composite comprising PC and 20 wt.% multi-walled carbon nanotubes (CNT) (NT-7; Hodogaya Chemical Co., Ltd., Japan)—i.e., PC/CNT (80/20 weight fraction ratio)—was kindly provided by Hodogaya Chemical Co., Ltd. in pellet form. The diameters of the CNTs ranged from 40 to 80 nm, and their lengths were between 10 and 20 μm. The density of the composite was approximately 2300 kg/m^3. Further details were described in the literature.[39-41]

Sample preparation

Prior to melt blending, pure PC and PC/CNT (80/20) were dried at 120 °C for 8 h in a vacuum oven to remove the moisture to avoid hydrolysis reaction.[12] PC/CNT (80/20), pure PC, and UHMWPE were mixed in a Labo-Plastmill internal batch mixer (Toyo Seiki Seisaku-syo, Ltd., Japan) at 250 °C for 20 min at a blade rotation speed of 50 rpm. The weight fractions of PC/CNT/UHMWPE were 60/8/32, 46/8/46, and 32/8/60, with 5000 ppm of Sumilizer-GP thermal stabilizer (Sumitomo Chemical Co., Ltd., Japan). The obtained samples were compressed into flat 1 mm-thick sheets using a table-type test press laboratory compression molding machine (Tester Sangyo Co., Ltd., Japan) at 250 °C and 10 MPa for 6 min, and subsequently cooled to 25 °C for 3 min.

Measurements

The temperature dependency of the dynamic tensile moduli was measured using a Rheogel-E4000 dynamic mechanical analyzer (UBM Co. Ltd., Japan) at 10 Hz between 100 and 220 °C at a heating rate of 5 °C/min. Rectangular 1 mm-thick specimens were cut from the compressed films.

Surface and volume resistivities of the sheets were evaluated using MCP-HT450 and MCP-T610 constant voltage-supplied resistivity meters (Mitsubishi Chemical Analytech Co.,

Ltd., Japan). The average value for each sample was calculated from nine measurements made at 23 °C.

The flat PC/CNT/UHMWPE sheets (each approximately 1 mm thick) were immersed in chloroform for 3 days at room temperature to remove the PC fraction. Then the insoluble portions were dried and weighed to determine the soluble fraction *S*, defined as follows:

$$S = \frac{w_i - w_f}{w_i} \times 100\,, \tag{3}$$

where w_i is the initial weight of the sample, and w_f is the weight of the dry insoluble portion. The insoluble part in chloroform was further immersed in xylene at 140 °C for 4 h to determine the weight fractions of soluble and insoluble portions in hot xylene.

A Spectrum 100 Fourier-transform infrared spectroscopy (FTIR) analyzer (Perkin Elmer, Inc., MA, USA) was used for the characterization. The soluble portions in chloroform and hot-xylene were used for the samples after drying.

The thermal properties of the samples were evaluated using a DSC8500 differential scanning calorimeter (DSC; Perkin Elmer, Inc.) under a nitrogen atmosphere. Each sample was heated from room temperature to 200 °C at a scanning rate of 10 °C/min to evaluate its heat of fusion and melting point (T_m). Then the sample was cooled to room temperature at 10 °C/min to evaluate the crystallization temperature (T_c).

The PC/UHMWPE morphology was observed using a TM3030Plus scanning electron microscope (SEM; Hitachi, Ltd., Japan). The cut surfaces of samples were immersed in aqueous solution of 15 wt.% of potassium iodide at 70 °C. Then, 5 wt.% of iodine was added and kept at 70 °C for 4 h for staining. The energy dispersive X-ray analysis was also performed after drying.

The CNT distribution was observed using an S4100 SEM (Hitachi, Ltd., Japan). Prior to observation, all specimens were coated with OsO_4 by a sputter coating machine. The surface of chloroform-insoluble portions and that of the cryogenically fractured ones were used.

RESULTS AND DISCUSSION

Effect of blend ratio

Initially, the dynamic mechanical properties were evaluated for binary blends of PC and UHMWPE at various blend ratios without CNTs. The temperature dependencies of the dynamic tensile moduli—i.e., the storage modulus E' and the loss modulus E''—are shown in Fig. 1 (a). Because the melting point (T_m) of UHMWPE is around at 135 °C (as shown later) and the glass transition temperature (T_g) of PC is approximately 165 °C, blends with a co-continuous structure must show step-wise decreases in the E' curve at both the T_m of UHMWPE and the T_g of PC.

As shown in Fig. 1 (a), there were almost no changes in E' or E'' at the T_m of UHMWPE for PC/UHMWPE (65/35), suggesting that UHMWPE was the dispersed phase while PC was the continuous one due to the huge viscosity difference. In contrast, there was a stepwise decrease in the E' of PC/UHMWPE (50/50), although the modulus drop at T_m was not so obvious. This result was expected because a large portion of the PC, which had a lower viscosity, must have formed a continuous phase in this blend. In the case of PC/UHMWPE (35/65), there was a clear stepwise decrease in E' and a distinct peak in the E'' curve at the T_g attributable to PC. Beyond the T_g of PC, the blends containing large amounts of UHMWPE—i.e., PC/UHMWPE (50/50) and PC/UHMWPE (35/65)—exhibited a plateau region in the moduli curves, suggesting that UHMWPE formed a continuous phase. PC must also have formed a continuous phase in these blends, because they exhibited a marked drop in the

modulus at the T_g of PC. These results suggest that PC/UHMWPE (50/50) and PC/UHMWPE (35/65) had co-continuous structures.

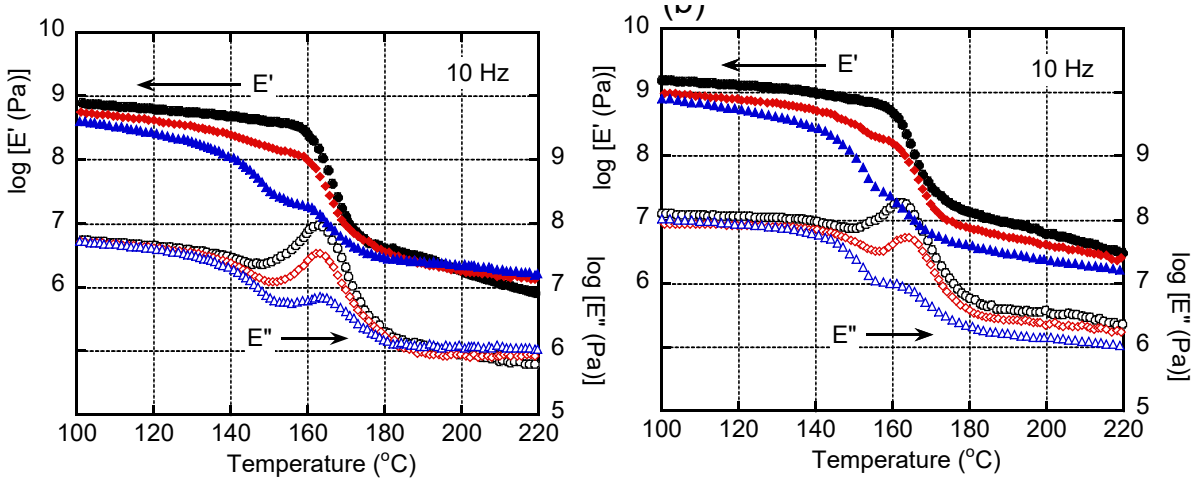

Fig. 1. Temperature dependence of dynamic tensile moduli such as (closed symbols) storage modulus *E'* and (open symbols) loss modulus *E"* for (black circles) PC/UHMWPE (65/35), (red diamonds) PC/UHMWPE (50/50), and (blue triangles) PC/UHMWPE (35/65): (a) without MWCNTs and (b) with MWCNTs (8 wt.%).

The dynamic mechanical properties for the composites with 8 wt.% CNT are shown in Fig.1 (b). The blend ratios of PC to UHMWPE were the same as those in Fig. 1(a). The dynamic mechanical properties were similar to those of the blends with enhanced moduli arising from the addition of rigid fillers, suggesting that PC/CNT/UHMWPE (46/8/46) and PC/CNT/UHMWPE (32/8/60) had co-continuous structures.

The melting of UHMWPE in the composites was clearly detected by the DSC measurements for all composites. As shown in Fig. 2, the peak temperatures of PC/CNT/UHMWPE (60/8/32), (46/8/46), and (32/8/60) in the first heating curve were located at around 133 °C. The heats of fusion, ΔH, were 56.8, 81.4, and 105.8 J/g, respectively.

Assuming that the heat of fusion of a perfect polyethylene crystal is 293 J/g,[42] the degrees of crystallinity per UHMWPE in the composites were around 60 wt.% for all composites.

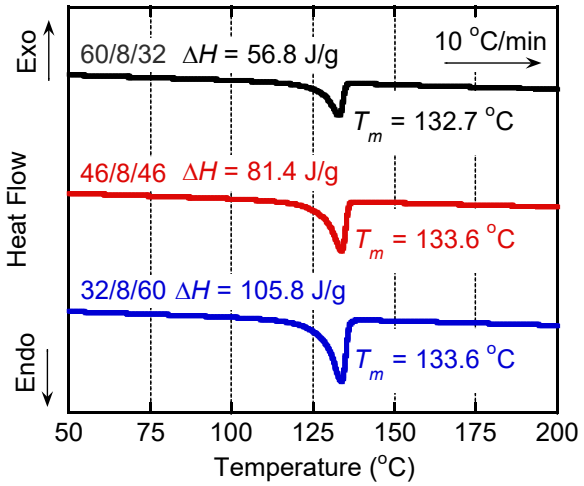

Fig. 2. DSC heating curves for PC/CNT/UHMWPE (60/8/32), (46/8/46), and (32/8/60) at 10 °C/min.

The effect of the CNT addition on the morphology was studied by SEM observation using the samples stained by iodine to differentiate PC and UHMWPE clearly. It was clarified by energy dispersion X-ray spectroscopy that the dark region is the PC phase. As seen in Fig. 3, co-continuous structures were detected for both samples, i.e., PC/UHMWPE (50/50) and PC/CNT/UHMWPE (46/8/46). Furthermore, the CNT addition was found to result in fine morphology, which is ascribed to the viscosity increase of the PC phase by CNTs.[40] The fine morphology attained by the CNT addition is reasonable, because the increase in the viscosity of the PC phase reduces the viscosity difference with UHMWPE. It is well-known that the viscosity matching plays an important role in the fine morphology of an immiscible polymer blend.[43-46] The CNT dispersion in the blend, which was unclear in Fig. 3 due to the low magnification, will be shown later.

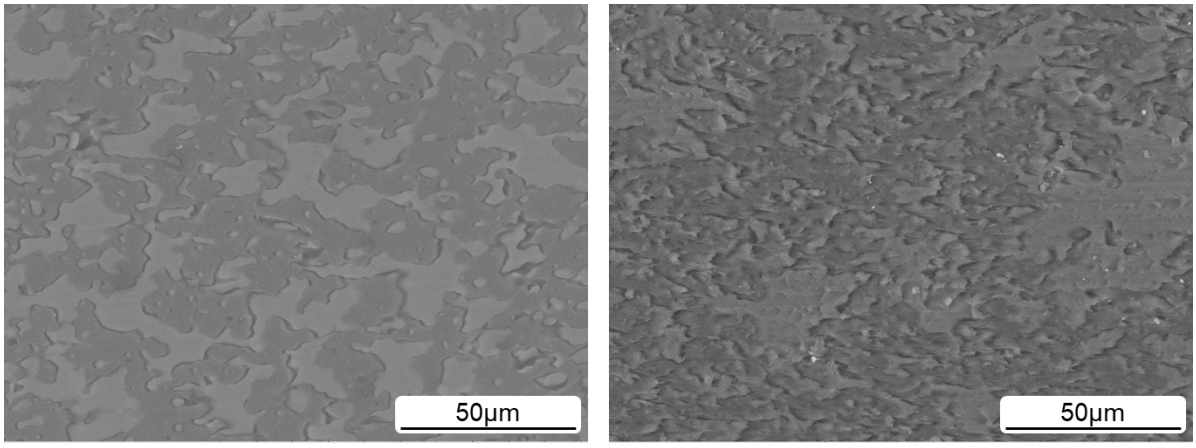

Fig. 3. Scanning electron microscope (SEM) images of cryofractured surface of (left) PC/UHMWPE (50/50) and (right) PC/CNT/UHMWPE (46/8/46) stained with iodine.

CNT dispersion in PC/CNT/UHMWPE

The immersion experiment using chloroform as a solvent was performed to determine the CNT dispersion. This is known to be a conventional method to characterize the structure of a polymer blend composed of a crystalline polymer and an amorphous polymer.[12,35,37] Photographs of the composites following immersion in chloroform are shown in Fig. 4. The weight fractions of the dissolved portion, which were confirmed as the PC fraction by FT-IR spectroscopy (Fig. 5), were measured after drying. The results were shown in Table 1. As seen in the table, the weight fractions of the soluble portions of PC/CNT/UHMWPE (60/8/32) and (46/8/46) were almost the same as the original weight fractions of the PC in those composites. However, that of PC/CNT/UHMWPE (32/8/60) was less than the original one of the PC. This is plausible because a part of PC covered with UHMWPE cannot be dissolved. As shown in Fig. 4, the solutions containing PC were fairly transparent as similar to PC/CNT/HDPE,[35] demonstrating that the CNTs were localized in the insoluble portion, i.e., the UHMWPE. Considering that the CNTs were mixed with the PC first, most of the CNTs transferred from the PC to the UHMWPE during mixing. According to our previous study, this is attributed to the surface adsorption of polyethylene chains on the CNT surface.[35]

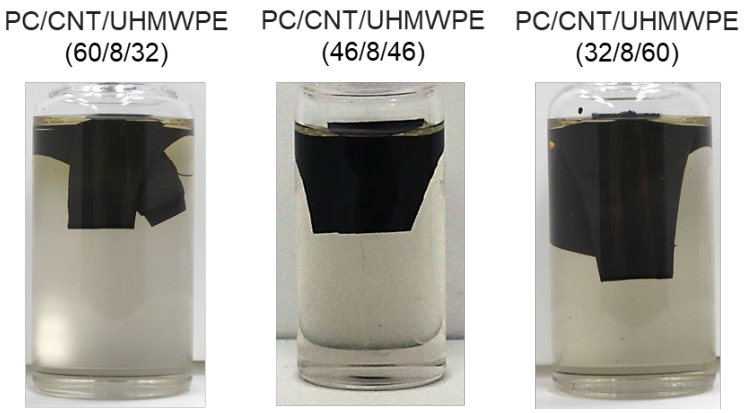

Fig. 4. Photographs showing the immersion of PC/CNT/UHMWPE (60/8/32), (46/8/46), and (32/8/60) in chloroform.

The insoluble parts in chloroform were further immersed in xylene at 140 °C for 6 h. Prior to the measurement, we confirmed that the UHMWPE was fully dissolved in the hot xylene. The solutions were found to be transparent and there was an insoluble part. The insoluble part must be composed of CNTs and polyethylene as demonstrated in our previous paper.[35] The weight contents of the xylene-insoluble part were slightly larger than those of the CNT in the composites.[35] Furthermore, the dissolved portions were confirmed as UHMWPE by the FT-IR spectroscopy (Fig. 5).

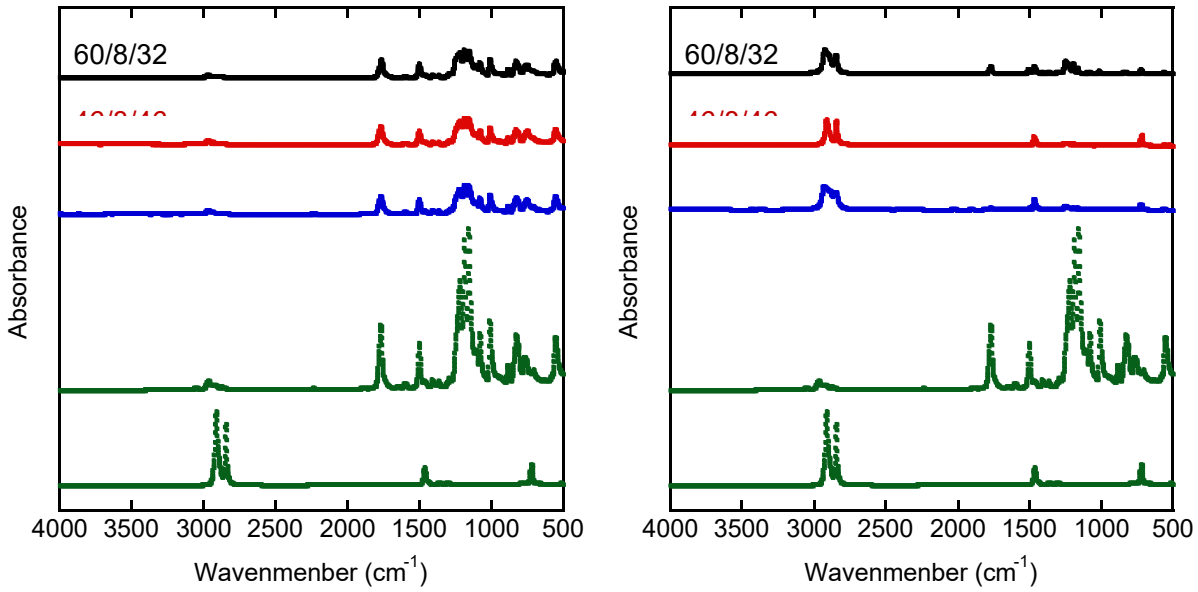

Fig. 5. FT-IR spectra of the soluble parts in (a) chloroform and (b) hot-xylene in PC/CNT/UHMWPE (60/8/32), (46/8/46), and (32/8/60), and those of the individual pure polymers.

Table 1. Insoluble/soluble parts in chloroform and hot-xylene

Samples	Soluble part in chloroform (wt.%)	Insoluble part in chloroform (wt.%)	
		Soluble part in hot-xylene (wt.%)	Insoluble part in hot-xylene (wt.%)
PC/CNT/UHMWPE (60/8/32)	62	29	9
PC/CNT/UHMWPE (46/8/46)	44	45	11
PC/CNT/UHMWPE (32/8/60)	25	59	16

The thermal properties of the insoluble portions in hot xylene were evaluated after vacuum drying to confirm the FT-IR results. The DSC heating and cooling profiles are shown in Fig. 6, in which T_m and T_c of UHMWPE were detected in the insoluble portions. The T_c seems to be slightly higher than that of pure UHMWPE. This will be owing to the strong nucleating ability of CNTs.[47,48]

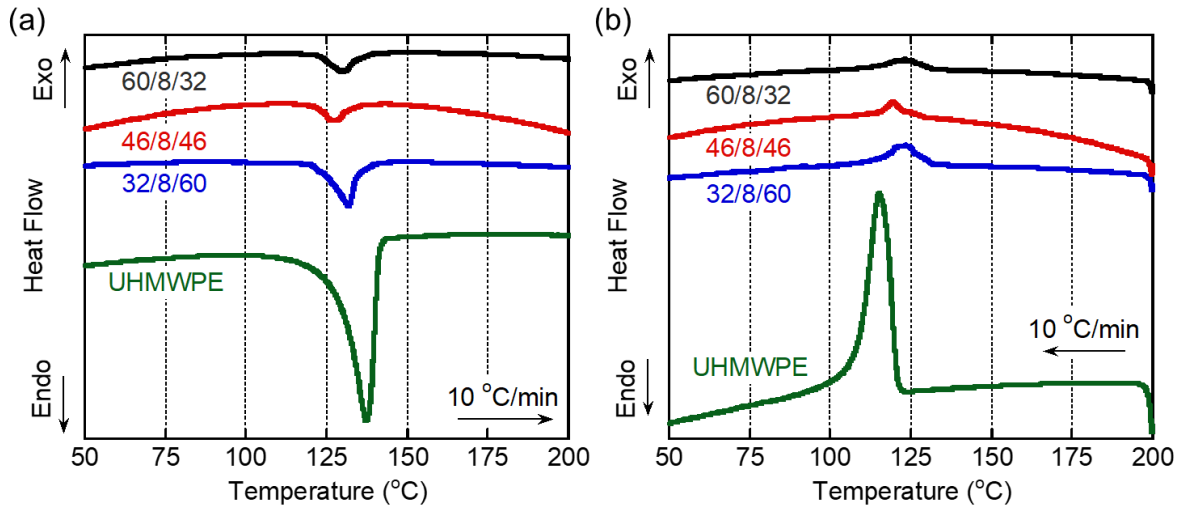

Fig. 6. DSC (a) heating and (b) cooling curves; insoluble portions in hot xylene of PC/CNT/UHMWPE (60/8/32), (46/8/46), and (32/8/60) with the data of pure UHMWPE. The heating and cooling rates were 10 °C/min.

The morphology of surface and inside of the insoluble portion in chloroform was investigated using SEM. To characterize the inside of the insoluble portions, the cryogenically fractured surface was used for the SEM observation. As shown in left pictures in Fig. 7, the CNTs were homogeneously distributed on the surface of the insoluble portions, i.e., the UHMWPE phase, irrespective of the blend ratios. In contrast, as shown in the right pictures in Fig. 7, it was impossible to confirm the presence of the CNTs on the fractured area denoted by an arrow, i.e., inside the UHMWPE phase. These results indicate that the CNTs were localized at the interface between the PC and the UHMWPE. According to our previous study,[35] in the case of PC/CNT/HDPE composites (M_n = 8.7 × 10^3 and M_w = 4.9 × 10^4 for HDPE), the CNTs were homogeneously distributed throughout the whole HDPE phase.

The diffusion constant of a particle is known to be inversely proportional to the viscosity of a medium. Since the molecular weight of the UHMWPE is almost 60 times higher than that of the HDPE used in the previous study, the zero-shear viscosity, which is proportional to $M^{3.4}$, is 1 x 10^6 times higher. Therefore, the diffusion coefficient of CNTs in

the UHMWPE must be 1 x 10^6 times lower than that in the HDPE.[38] Consequently, most CNTs were localized at the surface of the UHMWPE phase, as illustrated in Fig. 8.

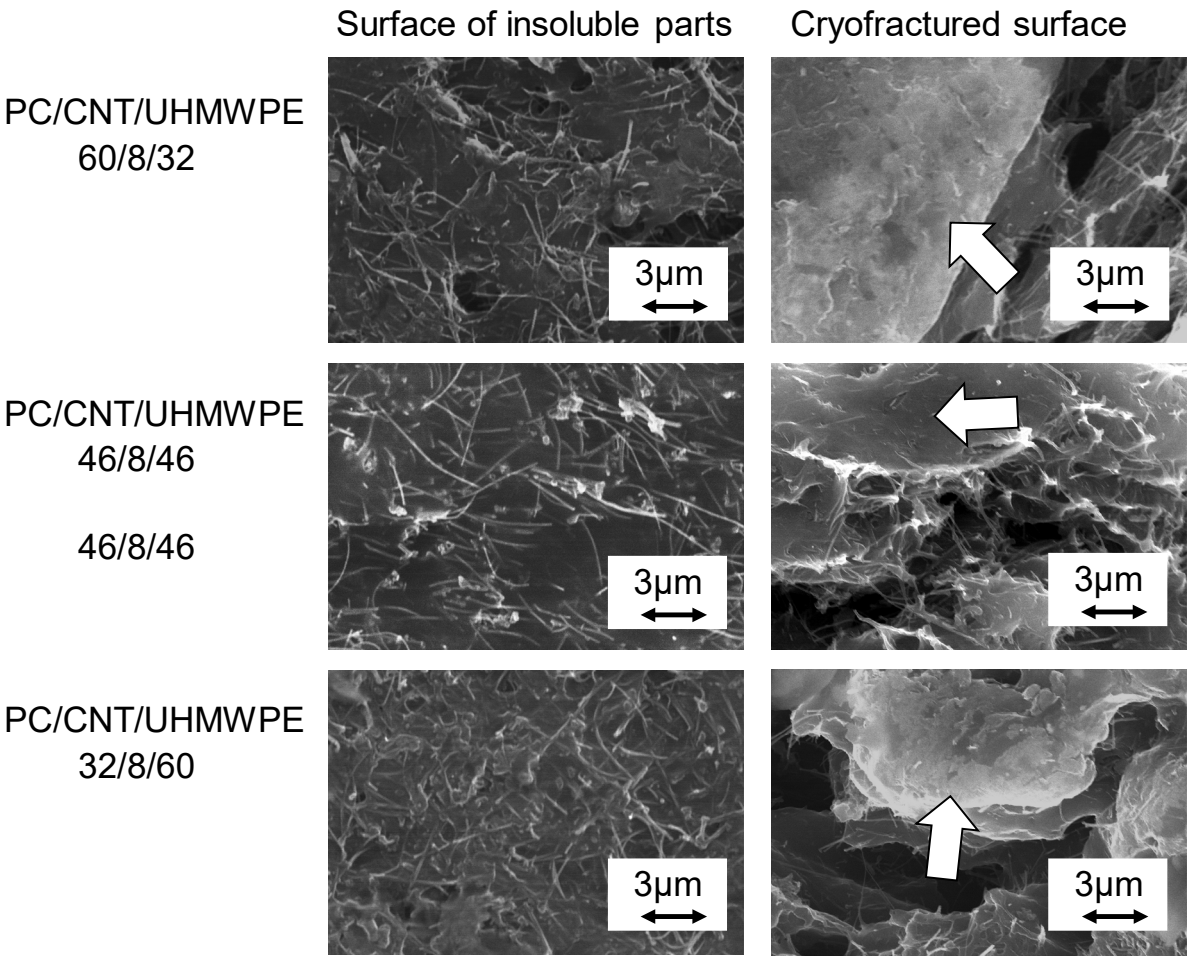

Fig. 7. Scanning electron microscope (SEM) images of (a) the surface and (b) the cryofractured surface of the chloroform-insoluble portion of PC/CNT/UHMWPE.

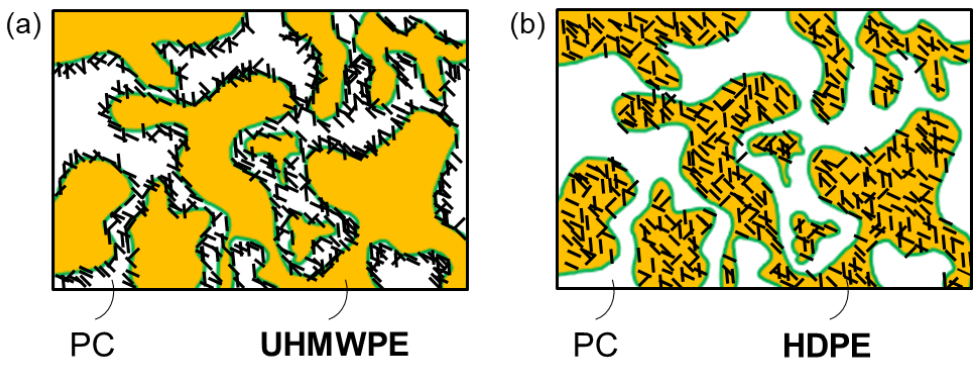

Fig. 8. Schematic illustration of CNT dispersion in (a) PC/CNT/UHMWPE (46/8/46) and (b) PC/CNT/HDPE (46/8/46).

Resistivity of PC/CNT/UHMWPE

The surface and volume resistivities are summarized in Fig.9. Although the surface and volume resistivities for the blends without CNTs were too high to be evaluated (> 1.0 x 10^{10} Ω/sq. for surface resistivity and > 1.0 x 10^{10} Ω cm for the volume resistivity), PC/CNT/UHMWPE (46/8/46) had good conductivity. This was expected because PC/CNT/UHMWPE (46/8/46) had a co-continuous structure with CNT localization at the phase boundary. The resistivities of PC/CNT/HDPE (46/8/46) were also evaluated as references, and found them to be markedly high (1.0 x 10^{10} Ω/sq. for the surface resistivity and > 10^{10} Ω cm for the volume resistivity). We conclude that composites containing UHMWPE have the potential to provide good electroconductivity.

Although the level of the electroconductivity in this study is not prominent as compared with recent advanced reports using the double percolation method (10^{1} – 10^{3} Ω cm for composites with 1-10 wt.% of CNTs),[10,11,13] it is presumably attributed to low electroconductivity of the CNT used in this study. It is well known that the electroconductivity is dependent upon the characteristics of CNTs.[1-6]

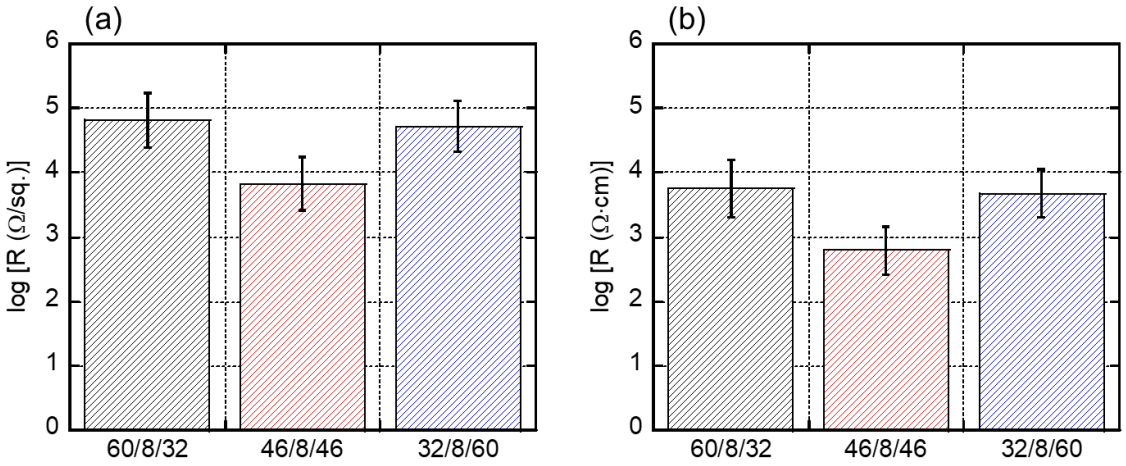

Fig. 9. (a) Surface and (b) volume resistivities for PC/CNT/UHMWPE.

CONCLUSIONS

In the present study, we investigated the structures and electroconductive properties of composites comprising PC, UHMWPE, and CNTs. Although the CNTs preferred the UHMWPE phase, they were localized on the surface due to a low diffusion constant of CNTs in UHMWPE. Because of the interphase localization, the blends with co-continuous structures have good electroconductivity owing to the presence of an electrically conductive path. The slow diffusion of CNTs is responsible for the peculiar CNT distribution, which can be applicable to various polymer blends having a high-viscosity component. From the viewpoint of thermodynamics, i.e., wetting coefficient, only limited blend systems exhibit the interphase localization of nanofillers. In fact, the CNT dispersion at interphase is not allowed at the equilibrium state also for the present blend systems, which can be predicted by the wetting coefficient. Therefore, the results obtained in this study will be important to widen the material design for conductive polymer blends. Moreover, the morphology control of this method is applicable to various nanocomposite systems.

ACKNOWLEDGMENT

A part of this work was supported by JSPS Grant-in-Aid for Scientific Research (B) Grant Number 16H04201.

REFERENCES

1. Kortschot, M. T.; Woodhams, R. T. *Polym. Compos.* **1985**, *6*, 296–303.
2. Grady, B. P., *Carbon nanotube - polymer composites*, Wiley, Hoboken, 2011.
3. Grossiord, N.; Hermant, M. C.; Koning, C. *Polymer carbon nanotube composites*, Pan Stanford Publishing, Singapore, 2012.
4. Tjong, S. C. *Polymer composites with carbonaceous nanofillers*, Wiley-VCH, Singapore, 2012.
5. Punetha, V. D.; Rana, S.; Yoo, H. J.; Chaurasia, A.; McLeskey, J. T.; Panasamy, M. S.; Sahoo, N. G.; Cho, J. W. *Progr. Polym. Sci.* **2017**, *67*, 1-47.
6. Pike, G. E.; Seager, C. H. *Phys. Rev. B* **1974**, *10,* 1421-1434.
7. Stauffer, D. *Introduction to percolation theory*, Taylor & Francis, London, 1985.
8. Sumita, M.; Sakata, K.; Hayakawa, Y. *Colloid Polym. Sci.* **1992**, *270*, 134–139.
9. Mamunya, Y. P. *J. Macromol. Sci. Part B* **1999**, *38*, 615–622.
10. Jia, L.; Yan, D.; Cui, C.; Ji, X.; Li, Z. *Macromol. Mater. Eng*. **2016**, *301*, 1232-1241.
11. Hosein, A.; Hoseini, A.; Arjmand, M.; S. Uttandaraman, Trifkovic, M. *Eur. Polym. J.* **2017**, *95*, 418-429.
12. Wiwattananukul, R.; Hachiya, Y.; Nobukawa, S.; Yamaguchi, M. *Polym. Compos*. **2017,** *38*, 1103–1111.
13. Poothanari, M. A.; Abraham, J.; Kalarikkal, N.; Thomas, S. *Ind. Eng. Chem. Res.* **2018**, *57*, 4287-4297.
14. Wu, S. *Polymer interface and adhesion*, Marcel Dekker, New York, 1982.

15. Sumita, M.; Sakata, K.; Hayakawa, Y. *Colloid Polym. Sci.* **1992**, *270*, 134–139.
16. Lee, B. L. *Polym. Eng. Sci.* **1992**, *32*, 36–42.
17. Chan, C.; Cheng, C.; Bay, C. W. *Polym. Eng. Sci.* **1997**, *37*, 1127–1136.
18. Grunlan, J. C.; Gerberich, W. W.; Francis, L. F. *J. Appl. Polym. Sci.* **2001**, *80*, 692–705.
19. Zhang, C.; Ma, C. -A.; Wang, P.; Sumita, M. *Carbon* **2005**, *43*, 2544–2553.
20. Doan, A. V.; Nobukawa, S.; Ohtsubo, S.; Tada, T.; Yamaguchi, M. *J. Polym. Research* **2013**, *20*, 145-150.
21. Wu, H.; Jia, L.; Yan, D.; Gao, J.; Zhang, X.; Ren, P.; Li, Z. *Compos. Sci. Technol*. **2018**, *156*, 87-94.
22. Zheng, L.; Li, Y.;Weng, Y.; Zhu, J., Zeng, J. *Compos. Part B, Eng*. **2019**, *167*, 683-689.
23. Iijama, S. *Nature* **1991**, *354*, 56–58.
24. Pötschke, P.; Fornes, T. D.; Paul, D. R. *Polymer* **2002**, *43*, 3247–3255.
25. Cecen, V.; Thomann, R.; Mülhaupt, R.; Friedrich, C. *Polymer* **2017**, *132*, 294–305.
26. Huang, Y.; Wang, W.; Zeng, X.; Guo, X.; Zhang, Y.; Liu, P.; Ma, Y.; Zhang, Y. *J. Appl. Polym. Sci.* **2018**, *135*, 46517.
27. Marcourt, M.; Cassagnau, P.; Fulchiron, R.; Rousseaux, D. *Polymer* **2018**, *157*, 156–165.
28. Soares, B. G.; Calheiros, L. F.; Silva, A. A. Indrusiak, T.; Barra, G. M. O.; Livi, S. *J. Appl. Polym. Sci.* **2018**, *135*, 45564.
29. Matos, M. A. S.; Pinho, S. T.; Tagarielli, V. L. *Scr. Mater.* **2019**, *166*, 117–121.
30. Adamson, A. W.; Gast, A. P. *Physical chemistry of surface*, Wiley, New York, 1997.
31. Ross, S.; Morrison, I. D. *Colloid systems and interfaces*, Wiley, New York, 1998.

32. Nuriel, S.; Liu, L.; Barber, A. H.; Wagner, H. D. Chem. *Phys. Lett.* **2005**, *404*, 263-266.

33. Regina, M.; Hamester, R.; Dalmolin, C.; Becker, D. *J. Appl. Polym. Sci.* **2019,** *136*, 48195.

34. Brandrup, J.; Immergut, E. H.; Grulke, E. A.; Bloch, D. R. *Polymer handbook*, 4th ed., Wiley, New York, 1999.

35. Wiwattananukul, R.; Hachiya, Y.; Endo, T.; Yamaguchi, M. *Compos. Part B, Eng.* **2015**, *78*, 409–414.

36. Wiwattananukul, R.; Fan, B.; Yamaguchi, M. *Compos. Sci. Technol.*. **2017,** *141*, 106–112.

37. Fan, B.; Wiwattananukul, R.; Yamaguchi, M. *Eur. Polym. J.* **2017**, *96*, 295–303.

38. Doi, M.; Edwards, S. F. *The theory of polymer dynamics*, Clarendon Press, Oxford. 2004.

39. Yoon, H.; Okamoto, K.; Yamaguchi, M. *Carbon* **2009**, *47*, 2840–2846.

40. Yoon, H.; Okamoto, K.; Umishita, K.; Yamaguchi, M. *Polym. Compos*. **2011**, *32*, 97-102.

41. Nishikawa, R.; Yoon, H.; Yamaguchi, M. *Nihon Reoroji Gakkaishi* **2019**, *47*, 105-110.

42. Mandelkern, L.; Fatou, J. G.; Denison, R.; Justin, J. *J. Polym. Sci., Phys*. **1967**, *1*, 41-91.

43. Wu, S. *Polym. Eng. Sci.* **1987**, *27*, 335-343.

44. Favis, B. D.; Therrien, D. *Polymer* **1991**, *32*, 1474-1481.

45. Larson, R. G. *The structure and rheology of complex fluids*, Chap. 9, Oxford Univ. Press, New York, 1999.

46. Meijer, H. E. H.; Janssen, J. M. H.; Anderson, P.D. *Mixing of immiscible liquids*, in Ed. Manas-Zloczower, I. *Mixing and compounding of polymers*, 2nd ed., Chap. 3. Hanser: Munich, 2009.

47. Seven, K. M.; Cogen, J. M.; Gilchrist, J. F. *Polym. Eng. Sci.* **2016**, *56*, 541-554.

48. Nishikawa, R. Yamaguchi, M. *J. Appl. Polym. Sci.*, **2019**, *136*, 48010.